Available online at www.sciencedirect.com
SCIENCE DIRECT®
Electrochemistry Communications 6 (2004) 91–97
electrochemistry communications
www.elsevier.com/locate/elecom

A multi-electrode probe for parallel imaging in scanning electrochemical microscopy

Anna L. Barker [a,*], Patrick R. Unwin [a], Julian W. Gardner [b], Hugh Rieley [c]

[a] Department of Chemistry, University of Warwick, Coventry CV4 7AL, UK
[b] School of Engineering, University of Warwick, Coventry CV4 7AL, UK
[c] Unilever Research Port Sunlight Laboratory, Quarry Road East, Bebington, Wirral L63 3JW, UK

Received 28 August 2003; received in revised form 20 October 2003; accepted 20 October 2003

Abstract

The first use of a parallel (multiple data acquisition) electrode probe for amperometric imaging in scanning electrochemical microscopy (SECM) is described. A 16-electrode linear microdot device has been designed based on an array of 10 μm diameter disc electrodes with a pitch of 120 μm, that are individually addressable. This configuration leads to essentially no overlap of diffusion fields when this electrode is used for amperometric detection. Linear sweep voltammetry, together with fluorescence confocal laser scanning microscopy, has been used to assess the characteristics of the device. To demonstrate the possibilities of parallel imaging in SECM, we report use of the device to image a heterogeneous substrate with conducting and insulating features.

Keywords: Scanning electrochemical microscopy; Microdisc assay; Electrochemical imaging; Fluorescence confocal laser microscopy

1. Introduction

Scanning electrochemical microscopy (SECM) is a scanned probe microscopy (SPM) technique employing a mobile amperometric or potentiometric electrode to probe interfacial processes. In imaging applications, the probe electrode is generally scanned in an x–y plane above the interface of interest and the electrochemical response, recorded as a function of electrode position, is used to map a particular property of the interface. This approach has provided novel insights into a myriad of interfacial processes, including electron transfer [1–3], corrosion [4–6], dissolution phenomena [7,8], membrane transport [9–12], enzyme activity [13,14] and cellular activity [15,16], among many other applications reviewed in full elsewhere [17].

Many of the applications of SECM, hitherto, have used a single scanning probe to map the substrate of interest, which can lead to lengthy data acquisition times. There are comparatively few examples of the use of multi-electrode probes in SECM. Exceptions include double-barrelled electrodes (such as dual amperometric/amperometric [15,18] and amperometric/potentiometric probes [19]), a recent micro ring–disc probe [20,21] and a heptode [22], although the latter involved several electrodes in summation.

In this paper, we describe a parallel electrode probe that allows multiple data acquisition in SECM imaging with 16 individually addressable electrodes in a linear array. The motivation for the development of this SECM probe is that such a device permits large areas of a sample to be imaged on a faster timescale than with single electrodes. There are many instances when large scan images of an entire sample are of interest, such as determining the density of active or defect sites on oxide-coated metal surfaces [23]. Parallel SPM tips have found application in atomic force microscopy (AFM) [24,25], but, surprisingly, not yet in SECM. Static multi-electrode arrays have, however, been used for spatially resolved chemical measurements [26,27], but the pixel density is limited by the electrode size and the need for widely spaced electrodes to avoid the overlap of diffusion

* Corresponding author. Fax: +44-024-765-24112.
E-mail address: a.l.barker@warwick.ac.uk (A.L. Barker).

1388-2481/$ - see front matter © 2003 Published by Elsevier B.V.
doi:10.1016/j.elecom.2003.10.019

fields in parallel amperometric operation. The work in this paper is the first instance of scanned probe SECM imaging with a multi-electrode array, which permits large area imaging of a sample on a faster timescale than with single electrode probes.

2. Experimental

2.1. Materials

All solutions were prepared using ultrapure water (Millipore Corp, Watford, Herts, UK, resistivity >18 MΩ). For voltammetry and SECM experiments solutions contained 10 mM hexaaammineruthenium(III) chloride (Strem chemicals, Newburyport, MA) with 0.2 M potassium chloride (A.R. Fisher Scientific, Loughborough, UK) as supporting electrolyte. For confocal microscopy measurements solutions contained 1 mM of 1,4-benzoquinone (Aldrich), henceforth abbreviated as BQ, and 8 μM disodium fluorescein (98%, Sigma) with 0.1 M potassium chloride. The pH was adjusted to 5.5 by addition of 0.1 M hydrochloric acid (Sigma). Array electrode devices were cleaned prior to use by rinsing them sequentially with 1-propanol, ethanol and ultrapure water.

2.2. Manufacture of array electrodes

The array electrodes were custom-made by processing a set of single-side polished 4 in. diameter p-type silicon wafers. The devices were designed at Warwick University using Tanner Tools (USA) and a set of mask-plates manufactured for the silicon run. The process involved taking the wafers and depositing a passivation layer of 800 nm of oxide followed by 200 nm of nitride. A platinum layer (30 nm seeding layer of titanium; 130 nm of platinum) was then deposited, followed by a top passivation layer of low-stress nitride (200 nm). The final stage was to open up the contact pads and windows for the microdots and reference electrodes. The silicon wafers were diced into individual chips and mounted on a custom-made printed circuit board (PCB) package. The devices for fast parallel SECM imaging consisted of a linear array of sixteen 10 μm diameter microdots, with a spacing (pitch) of 120 μm. This spacing ensured essentially no overlap of the steady-state diffusion fields between neighbouring electrodes. Each microdot in an array was discrete and addressable via separate metal tracks and bond pads. For studies in aqueous media, the exposed bond pads on the device and PCB, along with the bonding wires, were encapsulated with a conventional epoxy resin (Permabond).

Visual inspection of electrodes was carried out using an Olympus BH2 light microscope equipped with a 3-CCD colour video camera (model KY-F55BE, JVC). Images were transferred to a PC using a Neotech (London) IGPCI image capture card. An image of a completed device is provided in Fig. 1(a), with a single microdot shown in detail in Fig. 1(b).

2.3. Instrumentation

The custom-built electrochemical instrumentation to control and measure the signals from the array devices comprised two transconductance amplifier cards and two voltage amplifier cards, each of eight channels. The transconductance capabilities were used for the experiments herein. The four cards were housed in a 3U high rack instrument case, along with a power supply unit and precision voltage source. The cards slotted into a backplane printed circuit board, where signals were routed to connectors that interfaced to a data acquisition card (National Instruments) in a portable computer. The mounted array electrode devices plugged into a custom-designed cable/connection box assembly that allowed the individual electrodes to be switched to open circuit when not in use. The connection box was attached to the main instrument via gold plated connector coaxial leads. Due to the high sensitivity of the operational amplifiers used, it was important to ensure that all parts of the instrument and cables were screened from electrical interference through connection to a common ground.

For electrochemical measurements, each Pt microdot on the array served as the working electrode in a conventional two-electrode arrangement with a silver quasi-reference electrode (AgQRE), against which all potentials are quoted, serving as a common reference. The potential of the AgQRE electrode was controlled with a purpose built triangular wave/pulse generator (Colburn Electronics, Coventry, UK) while the potential of the array electrodes was held at ground.

A substrate for SECM imaging experiments was produced by sealing a bundle of 50 μm Pt wires in a pulled borosilicate glass capillary and then polishing the end of the assembly flat, to reveal the surface shown in Fig. 2. This shows that four wires are exposed end on and one partly side on. SECM images of the (unbiased) substrate were recorded in feedback mode, using either a 10 μm diameter Pt microdisc electrode (ratio of insulator to electrode radius, $RG = 10$) or the array devices as the working electrodes. For the imaging array experiments, a cell was fabricated from a cut down polystyrene cuvette fixed around the array with epoxy resin. The solution contained 10 mM $Ru(NH_3)_6^{3+}$ as the chloride salt and 0.2 M KCl. As shown in Fig. 3, the scanning arrangement for these experiments differed from that usually employed in SECM, in that the array was stationary and the sample was mounted on a 3-axis piezo positioner that was used to translate the sample above the array. The electrochemical cell and electrodes were

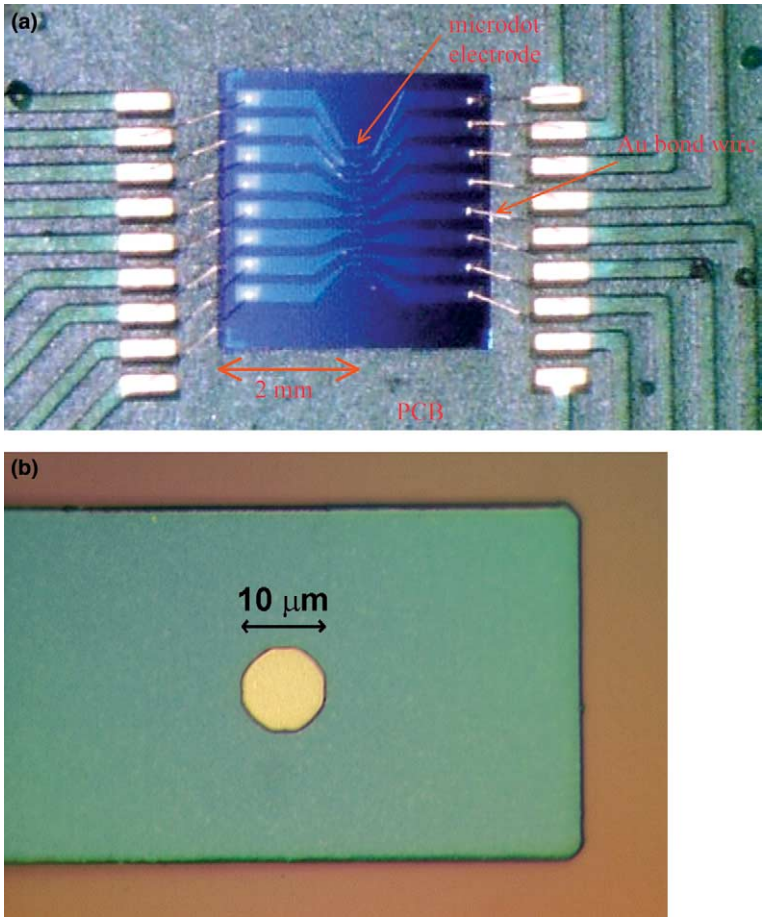

Fig. 1. Photograph of a linear array used for SECM imaging. (a) 10 μm diameter Pt microdots on a 16-electrode linear array. This figure shows exposed Au bonding wire connecting the contact pads on the device and on the PCB. (b) Optical micrograph of a microdot on the same device.

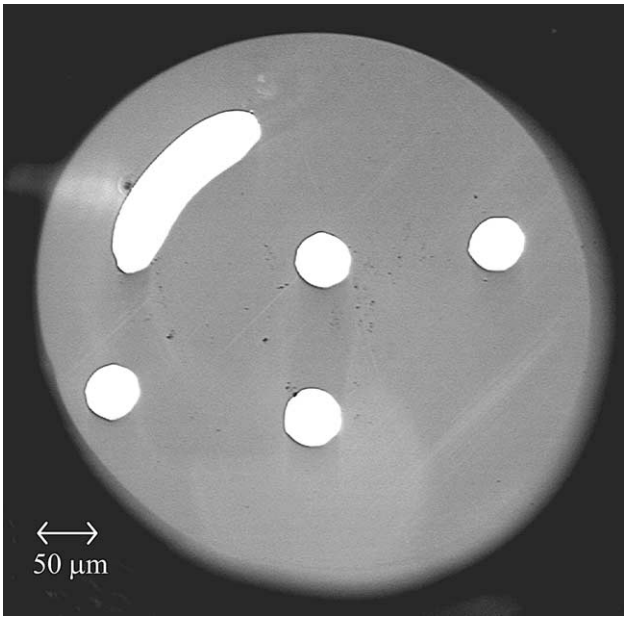

Fig. 2. Substrate used in test SECM imaging experiments produced by sealing a bundle of 50 μm Pt wires in glass.

shielded from electrical noise by a Faraday cage. All measurements were made at ambient temperature (23 ± 0.5 °C) in an air-conditioned room.

Images using combined electrochemical–confocal laser scanning microscopy (CLSM) were acquired with a Zeiss LSM 510, Axioplan 2, confocal microscope

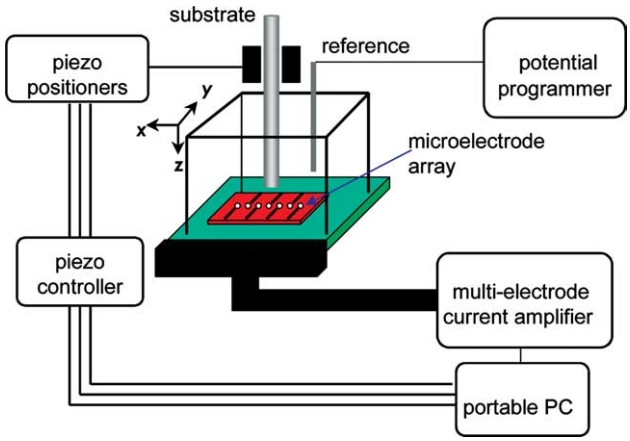

Fig. 3. Schematic showing the SECM set up used for parallel imaging.

equipped with an aqueous immersion objective (Zeiss Achroplan 20×/0.50 W) and a 10× tube lens. An Ar laser ($\lambda = 488$ nm) was used in conjunction with a long-pass filter ($\lambda = 505$ nm). Images were typically acquired by scanning an area of 650 μm × 650 μm in the x–y plane (parallel to the device). The confocal pinhole was set to give an optical slice of <4.4 μm to achieve adequate resolution and image intensity.

3. Results and discussion

3.1. Linear sweep voltammetry

The array electrodes, fabricated as described above, were demonstrated to be individually addressable by linear sweep voltammetry. Fig. 4 shows typical linear sweep voltammograms for all 16 of the 10 μm microdot electrodes on a linear array, for the one-electron reduction of $Ru(NH_3)_6^{3+}$ in a solution containing 10 mM $Ru(NH_3)_6Cl_3$ and 0.2 M KCl. The current at each electrode was recorded simultaneously, as the potential of the microdot was scanned with respect to the reference electrode from 0 to −0.6 V at a rate of 10 mV s^{-1}. The linear sweep voltammograms for the microdot electrodes exhibited the typical sigmoidal behaviour of conventional microelectrodes [28]. For each of the 16 electrodes tested the current approached a steady-state diffusion-limited value in the narrow range 13.2–13.7 nA at an applied potential, $E = -0.45$ V. This limiting current is lower than that measured for a 10 μm diameter/RG = 10 flat microdisc, for this solution, and is within 12 ± 2% of the value predicted for a microdisc recessed by the thickness of the insulating layer (200 nm) [29,30]. The deviation of the measured current from that predicted for recessed electrodes is probably due to the slight overlap of the edges of the diffusion profiles in bulk solution for the electrode–electrode separation used.

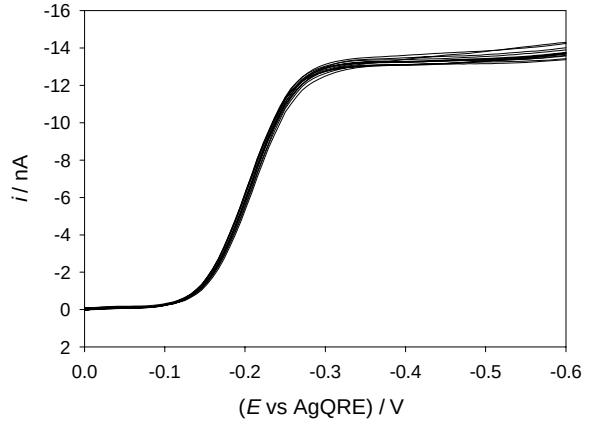

Fig. 4. Linear sweep voltammograms recorded at 10 mV s^{-1} for the reduction of 10 mM $Ru(NH_3)_6^{3+}$ in 0.2 M KCl at a linear array of sixteen 10 μm diameter Pt discs.

For some devices, several of the electrodes on the array initially gave lower steady-state currents than expected, suggesting that the electrodes may have been blocked by a contaminant arising from the fabrication process, that was not removed by the simple rinsing procedure. Several methods were examined to clean electrodes prior to use. One of the best strategies involved applying an anodic potential of +1.8 V for ~20 s. However, this procedure had to be used with care to ensure that it did not promote localised breakdown of the insulating silicon nitride layer.

Combined electrochemical – CLSM was used to reveal the activity of individual electrodes, through the electrochemical generation of pH profiles that were imaged by CLSM. This technique has recently been employed for 3D imaging of pH gradients at electrode surfaces with high spatial resolution [31]. The array was imaged using CLSM during the two electron–two proton reduction of BQ in an unbuffered solution containing disodium fluorescein, which exhibits a pH-sensitive fluorescence. The consumption of protons during the reduction of BQ to 1,4-hydroquinone at the electrodes results in a local rise in pH of the solution and enhanced fluorescence of the fluorescein. The method is a particularly sensitive means of highlighting the activity of an electrode.

Fig. 5(a) shows the linear sweep voltammograms obtained at 4 microdots on a linear device, when the potential of the electrodes was scanned from 0 to −0.4 V. Fig. 5(b) illustrates the corresponding fluorescence CLSM images at four different potentials from −0.1 V, at the foot of the BQ reduction wave, to −0.4 V, corresponding to the diffusion-controlled steady-state plateau. The images are for a plane ca. 5 μm above the surface of the array electrodes. The imaging parameters on the confocal microscope were selected to show the maximum contrast between the (low) initial background fluorescence of the solution at pH 5.5 and the intensity of the fluorescence generated around the microdots in the plateau region of the reduction wave. Fig. 5(b) clearly shows that there is a significant change in light intensity as function of applied potential. This is due to the increase in solution pH that results from two-electron, two-proton reduction of BQ, which causes fluorescein to fluorescence. Notice that the fluorescent zone expands to a similar size around each microdot as the potential of the electrodes is scanned to −0.4 V, indicating that there is a high degree of uniformity in the behaviour of the different electrodes. It is important to point out that the fluorescence profile is an indicator of the pH distribution. Thus, the size of the fluorescence profile at the diffusion-limited potential is much larger than the diffusion field at a microdisc electrode, where 90% of the bulk concentration would be recovered at distance ca. 6 electrode radii from the electrode centre [32].

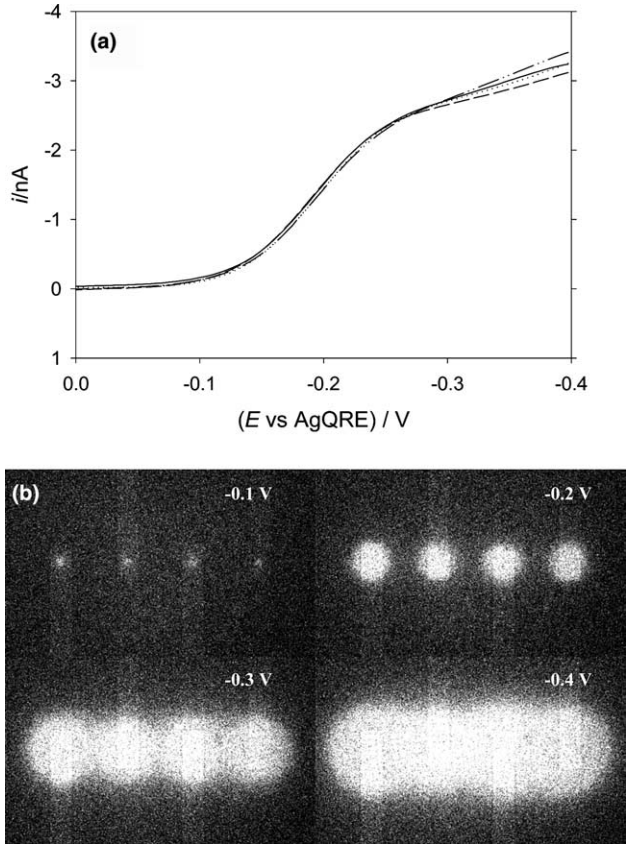

Fig. 5. (a) Linear sweep voltammograms recorded at 10 mV s^{-1} for the reduction of 1 mM benzoquinone in 8 μM disodium fluorescein solution at 4 microdot electrodes of a linear array and (b) CLSM images of fluorescence profiles (image size 566 μm × 344 μm) for the four microdot electrodes recorded at the potentials shown.

For the specific application of using the individually addressable microelectrode array as an amperometric SECM probe for parallel imaging, it was important to use the smallest possible thickness of silicon nitride on the array devices so that they were not recessed significantly. The greater the extent to which the electrodes are recessed, the smaller the current response and slower the time response [29,30]. On the other hand, the use of a thin insulating layer can compromise the long term stability of the electrode due to defects in the passivating layer and the poor corrosion characteristics of typical passivating materials, particularly in electrolyte solution [33]. Growth of the insulating film on step structures such as the edges of the conducting tracks is prone to being irregular and nodular and can lead to intrinsic stress, particularly pinhole defects along the track edges when thin insulating layers (<1 μm) are employed [33]. For the images in Fig. 5(b) there was no detectable increase in fluorescence intensity over areas of the array other than the microdots themselves, indicating that the device was free from defects in the insulating silicon nitride layer. The voltammetric responses of all the electrodes shown in Fig. 5(a) are similar and the steady state currents agree closely with the value expected. This again suggests that there are no pinholes in the insulating layer, exposing the underlying conducting tracks at which electrochemistry could take place.

3.2. High speed SECM imaging with a parallel 16-electrode linear array

Initially the substrate was imaged in a conventional SECM feedback set up using a 10-μm diameter Pt UME as the imaging tip. The tip/substrate distance was ca. 2–2.5 μm, as deduced from the current recorded at the tip for the diffusion-limited one-electron reduction of $Ru(NH_3)_6^{3+}$ as the probe was translated towards part of the insulating glass region of the substrate [34]. For imaging, the UME was raster scanned across the substrate at a rate of 10 μm s^{-1} with steps of 10 μm between each line. The total acquisition time to acquire a 500 × 500 μm square image was >2500 s. Typical data are shown in Fig. 6. The features observed were similar to those detected by the imaging array electrode, for which the results are reported below.

The set up used for parallel SECM imaging experiments was described earlier. To position the sample close to the imaging probe, the sample was translated towards the device. The individual currents measured at those array electrodes positioned directly under the substrate decreased to ~30% of the currents recorded with the substrate far (>500 μm) from the device indicating that they were in the vicinity of the insulating part of the substrate [34]. Under these conditions, the current was found to attain a quasi-steady response governed by the timescale of the procedure (20–30 s) and the distance

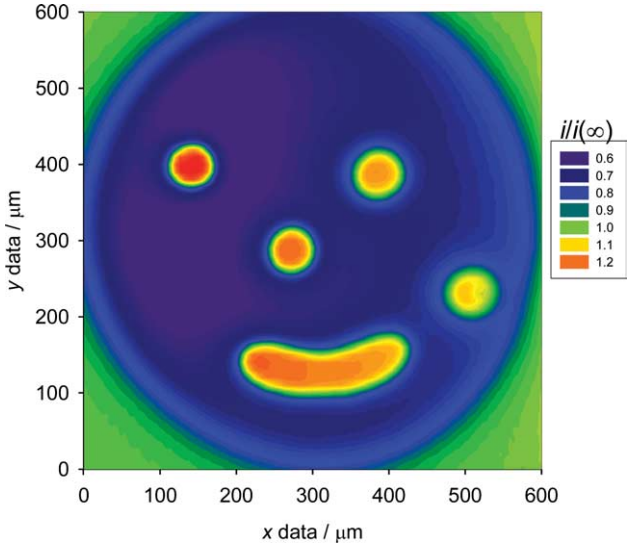

Fig. 6. SECM image of the substrate shown in Fig. 2 acquired in feedback mode using a 10 μm diameter Pt, RG = 10, UME tip. The tip current is normalised relative to the current measured at the tip in bulk solution, $i(\infty) = 16.2$ nA.

was estimated as 10 ± 5 μm. Over much longer times, the current at many of the electrodes would be expected to decay towards zero, since the effective RG values of the electrodes is very large compared to a conventional SECM single electrode probe [34]. The timescale for this process is governed by the overall dimensions of the linear array, l (~1 mm), which is large compared to typical tip/substrate separations, and is of order l^2/D, where D is the diffusion coefficient of the mediator (timescale typically $>10^3$ s).

Once the initial positioning of the tip was complete, images of the sample were obtained by measuring the diffusion-limited current response of all 16 electrodes (applied potential of −0.5 V), as the substrate was raster scanned laterally across the device. A scan rate of 10 μm s^{-1} was again employed, with steps of 10 μm between lines. Each line was 500 μm in length and corresponded to the y-axis in Fig. 3, with the microelectrode array oriented as shown in that figure. Each electrode recorded 12 lines, giving an overall area of 1910 μm × 500 μm. Fig. 7 shows a composite current image of the response of 5 neighbouring electrodes (those that sensed the sample). In this figure, the current response of each electrode has been normalised by the bulk current recorded for that particular microdisc on the array. The other electrodes measured were positioned beyond the edges of the sample. The area of 500 × 590 μm illustrated was imaged with a scan time that was about one-fifth of that required for a conventional probe.

Comparing Fig. 7 with Fig. 3, it can be seen that the SECM imaging technique readily identifies the active areas of the substrate. The current at each electrode, i, normalised with respect to the corresponding bulk steady-state current, $i(\infty)$, depends on whether the electrode is over the part of the substrate comprising inert insulating glass (current ratio, $i/i(\infty)$, in the range 0.3–0.4), or the metal surface (current ratios of ca. unity). Note that as in Fig. 6, the latter values are smaller than for diffusion-limited positive feedback [34], because the unbiased substrate has a finite size [1,35,36]. It is clear from the image in Fig. 7 that the device and substrate are oriented parallel to one another with a high degree of precision. The small difference in the feedback currents over the conducting areas is mainly due to the slight tilt on the sample relative to the device, as also revealed by the background current over the insulating region. The currents recorded at the microdots over the insulating area of the substrate in Fig. 7 are much lower compared with the RG = 10 UME in Fig. 6, for a similar electrode–substrate separation. This is a consequence of the larger effective RG of the array device, whereas the feedback current over the conducting areas are relatively unaffected, as expected from theory [34]. This highlights the advantage of using such large RG devices for improving the contrast in SECM imaging between active and non-active regions. It is also important to notice that the image is seamless which, in large part, is a consequence of the high level of uniformity of the electrodes in the microfabricated devices. If handled carefully a single array could be used for imaging in several different experiments.

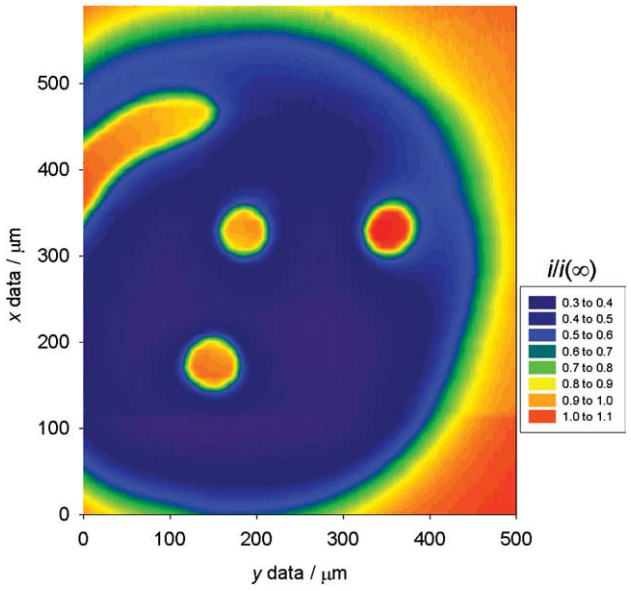

Fig. 7. SECM image of the substrate shown in Fig. 2, acquired simultaneously at 5 electrodes on the linear array, scanned in a direction perpendicular to long axis of device. Normalisation of the current at each microdisc is based on the individual responses of the electrodes in bulk solution.

4. Conclusions

Array electrodes, consisting of 16 individually addressable microdisc electrodes have been used for the first demonstration of parallel imaging in SECM. This approach allows larger scan images to be carried out on a shorter timescale than conventional single probe measurements and is expected to be particularly powerful in mapping active sites on surfaces, as considered in this paper. The electrodes described are readily fabricated and show well-defined characteristics, based on both voltammetric measurements and fluorescence CLSM, which has highlighted the uniform response of the electrodes in this type of array. Further developments of the imaging array could include selective derivatisation of the electrode surfaces to permit multi-functional imaging with a single probe in both amperometric and potentiometric formats.

Acknowledgements

We thank Unilever Research, Port Sunlight Laboratory for funding. The contributions to this work by Ian

Griffith and Philip Roskelly (Electronics workshops of the Departments of Engineering and Chemistry, University of Warwick) are gratefully acknowledged. We also thank Dr Susan Cannan for helpful discussions.

References

[1] A.J. Bard, M.V. Mirkin, P.R. Unwin, D.O. Wipf, J. Phys. Chem. 96 (1992) 1861.
[2] M.V. Mirkin, T.C. Richards, A.J. Bard, J. Phys. Chem. 97 (1993) 7672.
[3] S.B. Basame, H.S. White, J. Phys. Chem. B 102 (1998) 9812.
[4] N. Casillas, S. Charlebois, W.H. Smyrl, H.S. White, J. Electrochem. Soc. 141 (1994) 636.
[5] J.W. Still, D.O. Wipf, J. Electrochem. Soc. 144 (1997) 2657.
[6] C.H. Paik, H.S. White, R.C. Alkire, J. Electrochem. Soc. 147 (2000) 4120.
[7] J.V. Macpherson, P.R. Unwin, J. Phys. Chem. 99 (1995) 3338.
[8] J.V. Macpherson, P.R. Unwin, J. Phys. Chem. 100 (1996) 19475.
[9] J.V. Macpherson, D. O'Hare, P.R. Unwin, C.P. Winlove, Biophys. J. 73 (1997) 2771.
[10] B.D. Bath, R.D. Lee, H.S. White, E.R. Scott, Anal. Chem. 70 (1998) 1047.
[11] M. Tsionsky, J. Zhou, S. Amemiya, F.-R.F. Fan, A.J. Bard, R.A.W. Dryfe, Anal. Chem. 71 (1999) 4300.
[12] N.J. Evans, M. Gonsalves, N.J. Gray, A.L. Barker, J.V. Macpherson, P.R. Unwin, Electrochem. Commun. 2 (2000) 201.
[13] D.T. Pierce, P.R. Unwin, A.J. Bard, Anal. Chem. 64 (1992) 1795.
[14] G. Wittstock, W. Schuhmann, Anal. Chem. 69 (1997) 5059.
[15] T. Yasukawa, T. Kaya, T. Matsue, Anal. Chem. 71 (1999) 4637.
[16] A. Hengstenberg, A. Blöchl, I.D. Dietzel, W. Schuhmann, Angew. Chem., Int. Ed. 40 (2001) 905.
[17] A.J. Bard, M.V. Mirkin (Eds.), Scanning Electrochemical Microscopy, Marcel Dekker, New York, 2001.
[18] J.E. Baur, H.M. Miller, M.A. Richardson, Anal. Chim. Acta 397 (1999) 123.
[19] C. Wei, A.J. Bard, G. Nagy, K. Toth, Anal. Chem. 67 (1995) 1346.
[20] P. Liljeroth, C. Johans, C.J. Slevin, B.M. Quinn, K. Kontturi, Electrochem. Commun. 2 (2002) 67.
[21] P. Liljeroth, C. Johans, C.J. Slevin, B.M. Quinn, K. Kontturi, Anal. Chem. 74 (2002) 1972.
[22] J. Ufheil, K. Borgwarth, J. Heinze, Anal. Chem. 74 (2002) 1315.
[23] I. Serebrennikova, S. Lee, H.S. White, Faraday Discuss. 121 (2002) 199.
[24] P. Vettiger, M. Despont, U. Drechsler, U. Durig, W. Haberle, M.I. Lutwyche, H.E. Rothuizen, R. Stutz, R. Widmer, G.K. Binnig, INM J. Res. Dev. 44 (2000) 323.
[25] S.H. Hang, C.A. Mirkin, Science 288 (2000) 1808.
[26] N. Kasai, Y. Jimbo, O. Niwa, T. Matsue, K. Torimitsu, Electrochemistry 68 (2000) 886.
[27] J. Pei, M.-L. Tercier-Waeber, J. Buffle, G.C. Fiaccabrino, M. Koudelka-Hep, Anal. Chem. 73 (2001) 2273.
[28] K. Aoki, K. Tokuda, J. Electroanal. Chem. 237 (1987) 163.
[29] A.L. Bond, D. Luscombe, K.B. Oldham, C.G. Zoski, J. Electroanal. Chem. 249 (1988) 1.
[30] P.N. Bartlett, S.L. Taylor, J. Electroanal. Chem. 453 (1998) 49.
[31] S. Cannan, I.D. Macklam, P.R. Unwin, Electrochem. Commun. 4 (2002) 886.
[32] R.M. Wightman, D.O. Wipf, in: A.J. Bard (Ed.), Electroanalytical Chemistry, vol. 15, Marcel Dekker, New York, 1989, p. 328.
[33] G. Schmitt, J.–W. Schultze, F. Faßbender, G. Buß, H. Lüth, M.J. Schöning, Electrochim. Acta 44 (1999) 3865.
[34] J. Kwak, A.J. Bard, Anal. Chem. 61 (1989) 1221.
[35] D.O. Wipf, A.J. Bard, J. Electrochem. Soc. 138 (1991) 469.
[36] J.V. Macpherson, C.J. Slevin, P.R. Unwin, J. Chem. Soc. Faraday Trans. 92 (1996) 379.